

PERIODIC CENTROIDAL VORONOI TESSELLATIONS

JINGYAN ZHANG, MARIA EMELIANENKO, AND QIANG DU

(Communicated by Steve L. Hou)

Abstract. Centroidal Voronoi tessellations (CVTs) are Voronoi tessellations whose generators coincide with the mass centroids of the respective Voronoi regions. CVTs have become useful tools in many application domains of arts, sciences and engineering. In this work, for the first time the concept of the periodic centroidal Voronoi tessellations (PCVTs) - CVTs that exhibit certain periodicity properties in the Euclidean space - is introduced and given a rigorous treatment. We discuss the basic mathematical structures of the PCVTs and show how they are related to the so-called CVT clustering energy. We demonstrate by means of a concrete example that the clustering energy can lose smoothness at degenerate points which disproves earlier conjectures about the CVT energy being globally C^2 -smooth. We discuss a number of algorithms for the computation of PCVTs, including modifications of the celebrated Lloyd algorithm and a recently developed algorithm based on the shrinking dimer dynamics for saddle point search. As an application, we present a catalog of numerically computed PCVT patterns for the two dimensional case with a constant density and a square unit cell. Examples are given to demonstrate that our algorithms are capable of effectively probing the energy surface and produce improved patterns that may be used for optimal materials design. The numerical results also illustrate the intrinsic complexity associated with the CVT energy landscape and the rich geometry and symmetry represented by the underlying PCVTs.

Key words. Centroidal Voronoi Tessellations, Periodic Centroidal Voronoi Tessellations, Clustering energy, Critical point, Saddle point, Lloyd's algorithm, Shrinking dimer dynamics, Complex energy landscape, Optimal material design.

1. Introduction

Centroidal Voronoi tessellations (CVTs) are Voronoi tessellations whose generators coincide with the mass centroids of the respective Voronoi regions [13]. Given their obvious geometric meaning, CVTs can be naturally viewed as a model and method for point distributions and spacial tessellations of regions/volumes in \mathbb{R}^d . Yet, they have also been generalized to many other spaces and abstract settings. Since the first comprehensive study on the subject published over a decade ago [13], the generality and universality of CVTs have turned them into a widely applicable tool in many subjects of science and engineering such as image processing and analysis, vector quantization and data analysis, resource optimization, optimal placement of sensors and actuators for control, mobile sensing networks, logistics system, cell biology and territorial behavior of animals, phyllotaxis, geophysical flows, optimal materials design, model reduction, point sampling, numerical quadrature, mesh generation and optimization, meshless computing, and numerical partial differential equations, see for instance, [1, 4, 5, 7, 9, 13, 14, 15, 17, 18, 21, 25, 29, 34, 36, 37, 40, 45, 46]. At the same time, there has been much progress toward the development of efficient algorithms for the computation of CVTs [10, 11, 12, 13]. For a recent review on the subject, we refer to [16] where one may also find a more up-to-date list of references.

Received by the editors June 1, 2011 and, in revised form, July 13, 2011.
2000 *Mathematics Subject Classification.* 65D18, 49M20, 65Z05.

In this work, we consider a special type of CVTs in the Euclidean space, namely, the periodic centroidal Voronoi tessellations (PCVTs). These special CVTs satisfy certain additional properties that make them periodic in space with respect to some unit cell. A rigorous definition and some of the related mathematical properties are given later, together with some discussions on the computation of PCVTs. It is easy to see that much of the general theory and algorithms developed for CVTs can be applied to PCVTs. For example, after some necessary modifications, an energy functional (which is often the CVT energy or the clustering energy) can be defined so that its critical points correspond to PCVTs. Such an energy functional has played an important role in the computation of CVTs, as it helps turning the computation of CVTs into a problem of nonlinear optimization. Indeed, for general CVTs, it is well-known that they correspond to critical points of the associated CVT clustering energy.

Our studies of PCVTs in the Euclidean space are motivated by a number of considerations. On one hand, with the spatial periodicity, PCVTs may have independent interests such as in the *latinized* CVT design [42] and in materials design that can take advantage of the symmetry and periodicity [43]. PCVTs also provide good examples to understand the interplay of geometry and symmetry in determining the energy landscape of the CVT clustering energy both near equilibrium states and near metastable or unstable transition states. Indeed, except in very special cases [33], the CVT energy is not convex in general. While the local equilibria of the energy are often of interest in most applications, the saddle points provide useful information on the energy barriers and the transition path. In fact, such saddle points might correspond to local minimizers of the energy subject to certain constraints. On the other hand, PCVTs are closely related to CVTs in the conventional sense as defined in [13]. In fact, according to the well-known Gershgorin's conjecture, one may speculate that as the number of generators gets large, locally all CVTs minimizing the energy would exhibit self-similar and periodic structures associated with the basic optimal Voronoi cells [26]. In two dimension, it was shown that such a cell is a regular hexagon [38] which is space tiling and forms a special PCVT in \mathbb{R}^2 . The dual Delaunay triangulation leads to the tessellation formed by regular triangles which also serves as an optimal triangulation by many criteria. In three dimension, compelling numerical evidence also supports the conjecture [19] with the basic cell given by the truncated dodecahedron and the corresponding CVT forming a BCC lattice, which is again a special PCVT in \mathbb{R}^3 . The dual triangulation is formed by the so called Sommerville tetrahedron which is understandably different from the regular tetrahedron as the latter is not space tiling. In addition to the facts mentioned above, the popular lattice based quantizer design [3] also leads to PCVTs corresponding to a constant density.

All of the above provides sufficient motivation for us to undertake a study of the periodic CVTs and their properties, which is the focus of this work. The paper is organized as follows. In Section 2 we formalize the concept of PCVT, illustrate them with several examples and relate them to the regular CVTs by means of the corresponding energy functional. Section 3 contains the discussion about the algorithms suitable to construct PCVTs and motivates the choice of a modification of the Shrinking Dimer Dynamics algorithm as a method of choice for this problem. We also discuss the question of energy smoothness and provide a counterexample showing that the energy can fail to be smooth at a degenerate point. We move on to provide a list of examples showing the local equilibria and saddle points of the

CVT clustering energy given by PCVTs in Section 4, which reveals the complexity of the CVT energy landscape never before explored in this context.

2. PCVT concept and properties

2.1. The CVT concept in \mathbb{R}^d . We first give the definition of CVTs in Euclidean space. To include the particular case of PCVTs in a natural way, we use a more general definition than those previously given in the literature [13, 16]. We begin with a given domain $\Omega \in \mathbb{R}^d$, possibly unbounded or for much of our focus, $\Omega = \mathbb{R}^d$, and a set of (possibly infinitely many) distinct points $\{\mathbf{x}_i\}_{i \geq 1} \subset \Omega$. For each point \mathbf{x}_i , $i \geq 1$, define the corresponding *Voronoi region* (or *Voronoi cell*) V_i , by

$$(1) \quad V_i = \{\mathbf{x} \in \Omega \mid \|\mathbf{x} - \mathbf{x}_i\| < \|\mathbf{x} - \mathbf{x}_j\| \text{ for } j \geq 1, j \neq i\},$$

where $\|\cdot\|$ denotes the Euclidean distance (the L^2 metric) in \mathbb{R}^d . Clearly $V_i \cap V_j = \emptyset$ for $i \neq j$, and $\bigcup_{i \geq 1} V_i = \Omega$ so that $\{V_i\}_{i \geq 1}$ is a *tessellation* of Ω . We refer to $\{V_i\}_{i \geq 1}$ as the *Voronoi tessellation* (VT) of Ω [39] associated with the point set $\{\mathbf{x}_i\}_{i=1}^n$. A point \mathbf{x}_i is called a *generator*; a subdomain $V_i \subset \Omega$ is referred to as the *Voronoi region* (or *Voronoi diagram*) corresponding to the generator \mathbf{x}_i . The generality considered here, in comparison with [13, 16], is that we allow the case of unbounded or infinite domains with possibly infinite number of generators (and thus Voronoi cells).

Given a density function $\rho(\mathbf{x}) \geq 0$ defined on Ω , for any bounded $V_i \subset \Omega$, the standard *mass center* (or *centroid*) $\mathbf{x}_i^* \in \Omega$ of V_i is given by

$$(2) \quad \mathbf{x}_i^* = \frac{\int_{V_i} \mathbf{x} \rho(\mathbf{x}) \, d\mathbf{x}}{\int_{V_i} \rho(\mathbf{x}) \, d\mathbf{x}}.$$

For any *bounded* region $V \subset \Omega$, the mass center or centroid of V can be equivalently defined by,

$$(3) \quad \mathbf{x}^* = \operatorname{argmin}_{\mathbf{y} \in V} \left\{ \int_V \rho(\mathbf{x}) |\mathbf{y} - \mathbf{x}|^2 \, d\mathbf{x} \right\}.$$

This allows various extensions which will be convenient to use here.

The usual definition states that a CVT is a special type of a Voronoi tessellation such that $\mathbf{x}_i = \mathbf{x}_i^*$, where $i = 1, \dots, N$ for some fixed number of generators $N > 0$. We want to extend this definition to the case of infinitely many generators, which requires a minor modification:

Definition 1. *Given the domain Ω , a Voronoi tessellation $\{(\mathbf{x}_i, V_i)\}_{i \geq 1}$ of Ω is called a *centroidal Voronoi tessellation* (CVT) if and only if all the Voronoi cells are bounded and the points $\{\mathbf{x}_i\}_{i \geq 1}$ which serve as the generators of the associated Voronoi regions $\{V_i\}_{i \geq 1}$ are also the centroids of those regions, i.e., if and only if $\mathbf{x}_i = \mathbf{x}_i^*$ for $i \geq 1$.*

Similarly as in [13, 14, 16], we may define the corresponding dual triangulation as the *centroidal Voronoi Delaunay triangulation* (CVDT) of the convex hull of the generators. Note that when Ω is bounded and the number of generators is finite, the above definition is the same as the traditional one given first in [13].

A generic Voronoi tessellation does not satisfy the CVT property in general; see Figure 1 for an illustration. On the other hand, given a density ρ and a number of

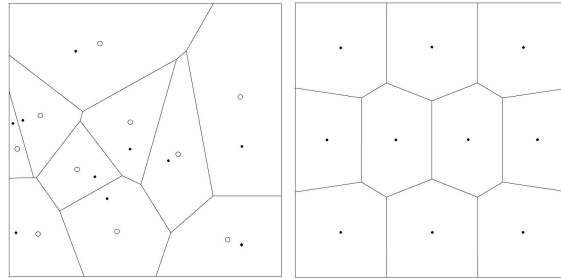


FIGURE 1. A Voronoi tessellation of the unit square with 10 randomly selected generators (the dots) which do not coincide with the centroids (the circles) and a 10-point centroidal Voronoi tessellation of the square for a uniform density [13].

generators n , the CVT of a bounded domain always exists though it may not be unique.

As a simple example of CVTs for unbounded domain, we can consider the uniform density and a uniform Cartesian rectangular mesh, together with the centers of all mesh cells, which forms a CVT in all of \mathbb{R}^2 . This in fact is a special case of the PCVTs which we define below.

2.2. PCVTs in \mathbb{R}^d . To consider PCVTs in the whole space $\Omega = \mathbb{R}^d$, let us first restrict our attention to periodic density functions.

Given a set of d linearly independent vectors $\{\mathbf{a}_i\}_{i=1}^d$ in \mathbb{R}^d , we define U , the corresponding *unit cell*, as

$$U = \{\mathbf{x} \in \mathbb{R}^d \mid \mathbf{x} = \sum_{i=1}^d x_i \mathbf{a}_i, \quad 0 \leq x_i < 1\}.$$

For convenience of notation, we define $\mathbf{A} = [\mathbf{a}_1, \mathbf{a}_2, \dots, \mathbf{a}_d]$.

The set $\{\mathbf{a}_i\}_{i=1}^d$ is named the *spanning vectors* (or *basis vectors*). A particularly simple but illustrative example that will be considered in our numerical simulations is the unit square in \mathbb{R}^2 spanned by two orthogonal unit vectors along the axes. Given a set (or domain) $V \subset \mathbb{R}^d$, and integer valued vector $\mathbf{k} = (k_i)_{i=1}^d \in \mathbb{Z}^d$, we use $V + \mathbf{A}\mathbf{k}$ to denote its translation with respect to U , that is,

$$V + \mathbf{A}\mathbf{k} = \{\mathbf{x} \in \mathbb{R}^d \mid \mathbf{x} = \mathbf{y} + \mathbf{A}\mathbf{k} = \mathbf{y} + \sum_{i=1}^d k_i \mathbf{a}_i, \quad \forall \mathbf{y} \in V\}.$$

A point set $\{\mathbf{x}_i\}_{i \geq 1}$ is said to be *translationally invariant* with respect to $\{\mathbf{a}_i\}$ if $\{\mathbf{x}_i\}_{i \geq 1} + \mathbf{A}\mathbf{k} = \{\mathbf{x}_i\}_{i \geq 1}$ for any $\mathbf{k} \in \mathbb{Z}^d$.

Definition 2. Given a unit cell U in $\Omega = \mathbb{R}^d$ with the spanning vectors $\{\mathbf{a}_i\}_{i=1}^d$, the set $\{(\mathbf{x}_i, V_i)\}_{i \geq 1}$ consisting generating points and a Voronoi tessellation of U is called a *periodic centroidal Voronoi tessellation (PCVT)*, with respect to U , if and only if $\{\mathbf{x}_i\}_{i \geq 1}$ is translational invariant with respect to $\{\mathbf{a}_i\}$ and U , and all the Voronoi cells are bounded and the points $\{\mathbf{x}_i\}_{i \geq 1}$ which serve as the generators of the associated Voronoi regions $\{V_i\}_{i \geq 1}$ are also the centroids of those regions, i.e., $\mathbf{x}_i = \mathbf{x}_i^*$ for $i \geq 1$.

In this work, we are only interested in the case when the set of generating points $\{\mathbf{x}_i\}_{i \geq 1}$ has a finite number of points $\{\mathbf{y}_i\}_{i=1}^n$ within the unit cell U , and we use n to represent the cardinality of such a generating set in U . The points $\{\mathbf{y}_i\}_{i=1}^n$ are called *generating points in the unit cell*. As an easy consequence we have

$$\{\mathbf{x}_i\}_{i \geq 1} = \bigcup_{\mathbf{k} \in \mathbb{Z}^d} (\{\mathbf{y}_i\}_{i=1}^n + \mathbf{A}\mathbf{k}) ,$$

that is, the set of infinitely many generators in the whole space is given by the periodic translations of those generating points in the unit cell. Moreover, without loss of generality, let $\{V_i\}_{i=1}^n$ be the Voronoi cells associated with $\{\mathbf{y}_i\}_{i=1}^n$ and let

$$(4) \quad U_i = U \cap \left(\bigcup_{\mathbf{k} \in \mathbb{Z}^d} V_i + \mathbf{A}\mathbf{k} \right) ,$$

we see that $\{U_i\}_{i=1}^n$ form a tessellation of the unit cell U and we may view them as the *periodic Voronoi regions* with respect to the unit cell U . For an illustration of the difference between the conventional Voronoi regions and the periodic Voronoi regions considered here for the same pair of generators in the unit square, we refer to Figure 2, where the shaded regions are associated with the first generator while the non-shaded ones with the second.

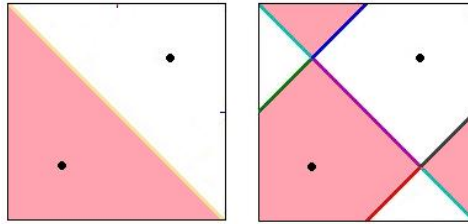


FIGURE 2. A standard Voronoi tessellation (left) of the unit square and a periodic Voronoi tessellation (right) of the unit square (as the unit cell) corresponding to the same pair of generators.

Finally, for any two points $\mathbf{x}, \mathbf{y} \in U$, let us define their U -distance, with respect to the unit cell as:

$$\|\mathbf{x} - \mathbf{y}\|_U = \min\{\|\mathbf{x} - \mathbf{y} - \mathbf{A}\mathbf{k}\|, \forall \mathbf{k} \in \mathbb{Z}^d\},$$

which measures the *true* distance with respect to the periodicity.

We are now ready to discuss various properties of PCVTs, some of which relate PCVTs to conventional CVTs while there are other properties distinguish PCVTs from CVTs.

2.3. Properties of PCVT. CVTs enjoy many nice features as shown in [13]. One may anticipate that many similar features can be shown for PCVTs as well. For instance, one of the nice features that helps making CVTs popular is the optimization property associated with CVTs which forms a basis for their various extensions and applications. For the PCVTs, we need to use suitable modifications to explore similar properties.

We first recall the clustering energy in the conventional sense. Given any set of points $\tilde{\mathbf{X}} = \{\tilde{\mathbf{x}}_i\}_{i=1}^n$ in a bounded Ω and any tessellation $\tilde{\mathbf{V}} = \{\tilde{V}_i\}_{i=1}^n$ of Ω , define

a CVT clustering energy by

$$(5) \quad \mathcal{K}(\tilde{\mathbf{X}}, \tilde{\mathbf{V}}) = \sum_{i=1}^n \int_{\tilde{V}_i} \rho(\mathbf{x}) \|\mathbf{x} - \tilde{\mathbf{x}}_i\|^2 \, d\mathbf{x}.$$

It can be shown that \mathcal{K} is minimized only if $\{(\tilde{\mathbf{x}}_i, \tilde{V}_i)\}_{i=1}^n$ forms a CVT of Ω . We remark that if $\{(\tilde{\mathbf{x}}_i, \tilde{V}_i)\}_{i=1}^n$ forms a CVT it does not necessarily minimize \mathcal{K} ; e.g., this set may correspond to a saddle point, as shown in [13]. The energy functional \mathcal{K} is often naturally associated with quantities such as *quantization error*, *variance* and *cost* in many applications.

To consider a similar energy for the PCVTs (or more generally, CVTs with infinitely many generators) the above form of \mathcal{K} would need to be modified. The reason for this is the fact that if infinitely many cells are allowed to contribute to the summation, a very restrictive condition on the density function would be needed in general to assure the convergence of the infinite series. Clearly, for PCVTs, it is more natural to consider the contributions to the energy of only those Voronoi regions that are associated with generators in the unit cell. In other words, for $\tilde{\mathbf{Y}} = \{\tilde{\mathbf{y}}_i\}_{i=1}^n$ and a tessellation $\tilde{\mathbf{V}} = \{\tilde{V}_i\}_{i=1}^n$ of the unit cell U we can define

$$(6) \quad \mathcal{K}_p(\tilde{\mathbf{Y}}, \tilde{\mathbf{V}}) = \sum_{i=1}^n \int_{\tilde{V}_i} \rho(\mathbf{x}) \|\mathbf{x} - \tilde{\mathbf{y}}_i\|_U^2 \, d\mathbf{x}.$$

Then, it is straightforward to see that

Proposition 1. *For a given positive integer n and a given unit cell U , let ρ be periodic with respect to U . Then the critical points of the PCVT energy \mathcal{K}_p correspond to PCVTs.*

While in principle the PCVTs have been defined slightly differently from the conventional CVTs, even on the same unit cell, there are still close connections between the two that one may explore. For instance, some PCVTs, when restricted to the unit cell, may happen to correspond to conventional CVTs of the same domain.

Proposition 2. *Given a periodic density function ρ defined with respect to a unit cell U , let $\{\mathbf{x}_i\}_{i \geq 1}$ be the generators of a PCVT that are obtained by a periodic translation of $\{\mathbf{y}_i\}_{i=1}^n$ located in the interior of U . If U consists of exactly a union of the corresponding Voronoi regions associated with $\{\mathbf{y}_i\}_{i=1}^n$, then it follows that these regions form a CVT of U in the conventional sense.*

On the other hand, from the CVTs defined in conventional sense, we may also construct PCVTs on larger domains. As illustration in the 2-dimensional space, let $\mathbf{D} = \text{diag}(-1, 1)$ denote a 2×2 diagonal matrix. Below we present a proposition which is easy to prove.

Proposition 3. *Consider a density function ρ defined on $U = [-1, 1]^2$, and let $\{\mathbf{x}_i\}_{i=1}^n$ be the generators of a CVT on U with respect to ρ that satisfy, in addition, the following two conditions:*

- i) all of them belong to the interior of U ,*
- ii) the set $\{\mathbf{x}_i\}$ is invariant under the mirror reflections in both x and y directions, i.e., $\{\mathbf{D}\mathbf{x}_i\}_{i=1}^n = \{-\mathbf{D}\mathbf{x}_i\}_{i=1}^n = \{\mathbf{x}_i\}_{i=1}^n$.*

Then $\{\mathbf{x}_i\}_{i=1}^n$ also represent the generators of a PCVT for the density which is a periodic extension of ρ with respect to U being the unit cell.

We note that the main argument for verifying the above proposition is to check the elementary geometric fact that under the symmetry properties, the conventional Euclidean distances of the points on the boundary of U to the generators are at the same time the U -distance defined earlier. This in turn implies that the Voronoi regions for each of the generators in the conventional sense are automatically the periodic Voronoi regions. Since the centroidal property remains the same, we obtain a complete equivalence between the CVT and PCVT in this case. For the constant density, some trivial examples of CVTs which are also PCVTs are given by Voronoi regions formed by uniform square lattices along with the cell centers as generators. A few less trivial examples of equivalent CVTs and PCVTs with respect to a two dimensional unit square and for a constant density are given in Figure 3.

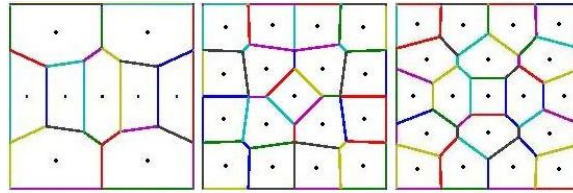


FIGURE 3. Some examples of CVTs with 9, 17 and 19 generators which are also PCVTs with respect to the unit square and a constant density.

Generally speaking, CVTs may not have the necessary mirror reflection symmetry assumed in the above proposition. Nevertheless, we can utilize geometric transformations to achieve such symmetry as demonstrated next.

Proposition 4. *Given a density function ρ defined on $U = [0, 1]^2$ and a 2×2 diagonal matrix $\mathbf{D} = \text{diag}(-1, 1)$, consider first an extension of ρ as an even function in both x and y directions to $U_1 = [-1, 1]^2$, then extend it periodically with U_1 as the unit cell. Take $\{\mathbf{x}_i\}_{i=1}^n$ to be the generators of a CVT in U with respect to the resulting density ρ that are located in the interior of U . Then the set $\{\mathbf{x}_i, \mathbf{D}\mathbf{x}_i, -\mathbf{D}\mathbf{x}_i, -\mathbf{x}_i\}_{i=1}^n$ forms a set of PCVT generating points in the unit cell U_1 . Moreover, the periodic Voronoi regions of $\{\mathbf{x}_i\}_{i=1}^n$ are the same as the conventional Voronoi regions.*

Examples of PCVTs formed via the above transformations of CVTs can be found in Figure 4. Again, a constant density is used.

PCVTs with respect to a given unit cell and spanning vectors may also inherit periodicity with respect to a different unit set and modified spanning vectors. It is partially for this reason that we have not required the use of a minimum unit set or an irreducible set of spanning vectors. For instance, PCVTs constructed on a unit cell given by a unit square may exhibit symmetry with respect to half of the square, see examples of such PCVTs in Figure 5.

3. Algorithms for Computing CVTs and PCVTs

Through the research in the past decade, there has been much progress in the development of efficient and robust algorithms for computing CVTs [10, 11, 32, 34, 41]

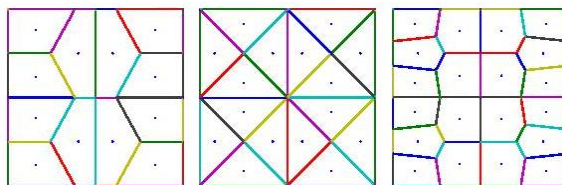


FIGURE 4. Examples of PCVTs which are formed by CVTs via mirror reflections and periodic extensions.

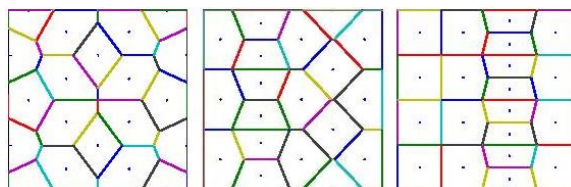


FIGURE 5. Examples of PCVTs (with 16, 18 and 20 generators in the unit cell given by a square) which are also periodic with respect to smaller unit cells (of size $1/2$, $1/3$ and $1/4$ respectively).

and their convergence analysis [11, 12, 25]. One popular method for computing CVTs corresponding to the minimum of the the CVT clustering energy is the celebrated Lloyd's algorithm [35] which can also be modified to compute the PCVTs. Over the years, a number of faster algorithms have been proposed, including linear parallel [32], multilevel algorithms [11] and nonlinear iterations such as the Lloyd-Newton algorithm [10]. To avoid the computation and storage of the Jacobian matrix in the Newton iteration, it was suggested in [13] that Newton-like or quasi-Newton method can be a better alternative. This is achieved with much success in a recent work of [34] based on the preconditioned *limited memory BFGS* (L-BFGS) method.

3.1. Non-smoothness of the energy at degenerate points. From the point of view of algorithmic development, especially for the validity of Newton-like methods, it is important to know whether the objective function is smooth. In the context of regular CVTs, this question was addressed in several recent studies. While it is not hard to show that the energy is locally C^2 near the critical points [13], its C^2 smoothness away from the critical points was only recently established in [34] through a detailed analysis. It was conjectured therein that the energy is globally C^2 everywhere in the computational domain. Here we provide a counterexample showing that the energy $\mathcal{E}(\mathbf{x}) = \mathcal{K}_p(\mathbf{x}, \mathbf{V}(\mathbf{x}))$ fails to be smooth at the points where two generators collapse (degenerate points). Let us take the example with $n = 2$ and a constant density $\rho \equiv 1$ defined on $U = [0, 1]^2$. By translation invariance, without any loss of generality, we may fix the first generator at $\mathbf{x}_1 = (0, 0)$. Now, consider the case where the second generator is at $\mathbf{x}_2 = (s, 0)$ with $s \in [0, 1]$, then

the energy $f(s) = \mathcal{E}((0, 0), (s, 0))$ is given as follows:

$$\begin{aligned} f(s) &= \int_{-\frac{1}{2}}^{\frac{1}{2}} \left\{ \int_{\frac{s-1}{2}}^{\frac{s}{2}} (z_1^2 + z_2^2) dz_1 + \int_{\frac{s}{2}}^{\frac{s+1}{2}} ((z_1 - s)^2 + z_2^2) dz_1 \right\} dz_2 \\ &= \int_{-\frac{1}{2}}^{\frac{1}{2}} \left\{ \int_{-\frac{1}{2}}^0 ((z_1 + \frac{s}{2})^2 + z_2^2) dz_1 + \int_0^{\frac{1}{2}} ((z_1 - \frac{s}{2})^2 + z_2^2) dz_1 \right\} dz_2 . \end{aligned}$$

Further simplification shows that

$$f(s) = \int_{-\frac{1}{2}}^{\frac{1}{2}} \int_{-\frac{1}{2}}^{\frac{1}{2}} (z_1^2 + z_2^2) dz_1 dz_2 - \frac{s(1-s)}{4} = \frac{2 - 3s + 3s^2}{12} .$$

Thus, we see that there could be three possible candidates for the critical points of the energy $\mathcal{E}((0, 0), \mathbf{x}_1)$: $s = 1/2$ which actually corresponds to a saddle point with

$$\frac{\partial}{\partial s} \mathcal{E}((0, 0), (s, 0)) \Big|_{s=\frac{1}{2}} = 0 ,$$

and the choice of $s = 0$ or $s = 1$ which corresponds to a local maxima where the two generators coincide to a single generator and satisfies

$$\lim_{s \rightarrow 0^+} \frac{\partial}{\partial s} \mathcal{E}((0, 0), (s, 0)) = - \lim_{s \rightarrow 1^-} \frac{\partial}{\partial s} \mathcal{E}((0, 0), (s, 0)) = -\frac{1}{4} \neq 0 .$$

Indeed, it is straightforward to see that for any \mathbf{x}_2 in U , we have

$$\mathcal{E}((0, 0), \mathbf{x}_2) \leq \lim_{\mathbf{x}_2 \rightarrow (0,0)} \mathcal{E}((0, 0), \mathbf{x}_2) = \int_{-\frac{1}{2}}^{\frac{1}{2}} \int_{-\frac{1}{2}}^{\frac{1}{2}} (z_1^2 + z_2^2) dz_1 dz_2 = \frac{1}{6} .$$

because of the inequality that, for any $\mathbf{y} \in U$,

$$\min\{\|\mathbf{y}\|_U, \|\mathbf{y} - \mathbf{x}_2\|_U\} \leq \|\mathbf{y}\|_U .$$

Thus, the clustering energy with two generators has a local maximum where the two points collapse onto a single point, as demonstrated also by the plot in the Figure 6 of the numerically computed energy $\mathcal{E}((0, 0), \mathbf{x}_2)$ with respect to the two coordinates of \mathbf{x}_2 .

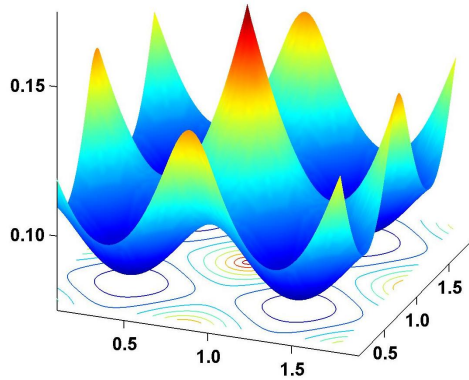


FIGURE 6. Plot of the PCVT energy with respect to the two coordinates of the second generator, showing a local maximum at $d = 0$ for the case of $\rho = 1, n = 2$.

However, the spatial gradients there do not vanish as computed in the above. Hence, we see that in the above example, the energy \mathcal{E} fails to be smooth at the degenerate points where $\mathbf{x}_1 = \mathbf{x}_2$, i.e.,

Proposition 5. *Let $\rho = 1$, $U = [0, 1]^2$ and $n = 2$. The PCVT clustering energy $\mathcal{E}(\mathbf{x}) = \mathcal{K}_p(\mathbf{x}, \mathbf{V}(\mathbf{x}))$ is not a C^1 function of the variable $\mathbf{x} = (\mathbf{x}_1, \mathbf{x}_2) \in U^2$ at the degenerate points $\mathbf{x} = (\mathbf{x}_1, \mathbf{x}_1)$ where two generators coincide.*

The calculation presented here is valid for both the original CVT and the PCVT given in the definitions 1 and 2 respectively. While the above proposition is provided for the simplest possible case of degeneracy, it serves as an illustration of a more fundamental phenomenon. The fact that the C^1 assumption fails even in such a trivial case implies that the PCVT (and CVT) energy cannot be expected to be smooth at degenerate locations in general, especially in more complicated situations where the density is not constant and the dimension and/or number of generators is increased.

3.2. Shrinking dimer dynamics (SDD) algorithm. As motivated above, we are interested in a comprehensive study of the energy landscape of the clustering energy. While the Newton-like iterations should work for the computation of a CVT or PCVT corresponding to any critical point, they are generally convergent only locally and with relatively small convergence balls for the initial guess. For more reliable and efficient computation of saddle points, especially those index-1 saddle points that often play a dominant role as transition states between local energy equilibria, there are other more sophisticated algorithms available. For example, the dimer method [30] was developed more than a decade ago to locate transition states of the given energy without the calculation of its Hessian. The dimer algorithm starts each iteration by a rotation step followed by a translation step through a careful combination of moves along both descending and ascending directions. The movement is reminiscent to the gentlest ascent method given in [8] and the continuous version of the latter studied in [24].

Recently, motivated by these earlier works, we developed a dynamical system for a shrinking dimer in [22] which provides a number of effective approaches to find index-1 saddle point of a given energy functional \mathcal{E} , which for the PCVT computation is taken to be $\mathcal{E}(\mathbf{x}) = \mathcal{K}_p(\mathbf{x}, \mathbf{V}(\mathbf{x}))$, where \mathbf{x} represents all generators in the unit cell U and $\mathbf{V}(\mathbf{x})$ is the associated Voronoi tessellation with respect to the U -distance.

Given an energy functional \mathcal{E} , and two feasible physical states represented by \mathbf{x}_1 and \mathbf{x}_2 with distance l , that is a so-called dimer with length l [30], let the negative gradient vector $-\nabla\mathcal{E}$ at those two points be denoted by \mathbf{F}_1 and \mathbf{F}_2 respectively, and let $\mathbf{x} = (\mathbf{x}_1 + \mathbf{x}_2)/2$ be the mid-point of \mathbf{x}_1 and \mathbf{x}_2 and \mathbf{v} be the unit vector $\mathbf{v} = (\mathbf{x}_1 - \mathbf{x}_2)/|\mathbf{x}_1 - \mathbf{x}_2|$. A particular form of the shrinking dimer dynamics (SDD) is given by the following system of ODEs [22]:

$$(7) \quad \begin{cases} \mu_1 \dot{\mathbf{x}} = (I - 2vv^T)(\mathbf{F}_1 + \mathbf{F}_2)/2, \\ \mu_2 \dot{\mathbf{v}} = (I - vv^T)(\mathbf{F}_1 - \mathbf{F}_2)/l, \\ \mu_3 \dot{l} = -\gamma(l), \end{cases}$$

where $\dot{\mathbf{x}}$, $\dot{\mathbf{v}}$ and \dot{l} denote time derivatives and $\{\mu_i\}_{i=1}^3$ are three non-negative time relaxation constants. In (7), the last equation for l controls the dimer length dynamically so that as time goes to infinity, the dimer length would approach zero, hence

the name *shrinking dimer dynamics*. A sufficient condition is to take $\gamma = \gamma(l)$ as the derivative of a smooth non-negative convex function $\Gamma = \Gamma(l)$ with $l = 0$ being the unique minimum. Here, we restrict attention to the special form of $\Gamma(l) = l^2/2$ associated with $\gamma(l) = l$, which corresponds to an exponential reduction of the dimer length in time.

For the clustering energy, the gradient vector \mathbf{F} can be conveniently computed based on the Lloyd map $\mathbf{L} = (\mathbf{L}_1, \dots, \mathbf{L}_n)^T$, which denotes the map between generators and the centroids of the associated Voronoi regions and is given by

$$(8) \quad \mathbf{L}_i(\mathbf{X}) = \frac{\int_{V_i(\mathbf{X})} \mathbf{x}\rho(\mathbf{x}) \, d\mathbf{x}}{M_i}$$

where

$$M_i = \int_{V_i(\mathbf{X})} \rho(\mathbf{x}) \, d\mathbf{x},$$

and $V_i(\mathbf{X})$ denote the Voronoi regions corresponding to the generators \mathbf{x}_i . For the case of PCVTs, we may simply use the periodic Voronoi regions $\{\tilde{V}_i\}$ as specified by (4) for each of the generators inside the unit cell U . The gradient operator of \mathcal{E} in component-wise form is then given by $2M_i(\mathbf{x}_i - \mathbf{L}_i(\mathbf{X}))$ (see [13] for some relevant discussion regarding standard CVTs, which remains valid when the periodic Voronoi tessellations are used). A detailed algorithmic analysis of the convergence and various implementation issues of the shrinking dimer dynamics and its time discretizations can be found in [22].

3.3. SDD method for PCVT. It turns out that a modification of the shrinking dimer dynamics may be better suited for the PCVT computation. This is due to the translational invariance of the PCVTs, together with the generators/centroids and the associated Voronoi regions. To eliminate such extra degrees of freedom, a constraint can be introduced. For instance, we may require that for the set of generators $\{y_i\}_{i=1}^n$ in the unit cell,

$$(9) \quad G(\mathbf{y}) = \sum_{i=1}^n (\mathbf{y}_i - 0.5\mathbf{a}_i) = 0 .$$

To deal with the possible complications due to constraints in the study of complex energy landscape, a constrained shrinking dimer dynamics (CSDD) was also developed in [23] by utilizing a Lagrange multiplier formulation. This turned out to work well for the PCVT computation subject to the constraint (9).

For the particular constraint G given by (9), we have

$$\nabla G = \left(\begin{array}{cccc} I_d & I_d & \dots & I_d \end{array} \right)$$

which is a constant matrix of size $d \times nd$, consisting of n blocks of $d \times d$ identity matrices.

A special version of the CSDD associated with the linear constraint (9) is then given as follows:

$$\begin{cases} \mu_1 \dot{\mathbf{x}} = (I - 2vv^T)(P\mathbf{F}_1 + P\mathbf{F}_2)/2, \\ \mu_2 \dot{\mathbf{v}} = (I - vv^T)(P\mathbf{F}_1 - P\mathbf{F}_2)/l, \\ \mu_3 \dot{l} = -l. \end{cases}$$

Here, the projection operator P is given by

$$(10) \quad P = I_{nd} - \nabla G^T (\nabla G \nabla G^T)^{-1} \nabla G = I_{nd} - I_d \otimes uu^T$$

with $u = (1, 1, \dots, 1)^T / \sqrt{n} \in \mathbb{R}^n$ being a unit vector. The initial conditions are required to satisfy (9) for the positions of generators in the unit cell which make up \mathbf{x}_0 and $P\mathbf{v}_0 = \mathbf{v}_0$. The implementation of the CSDD is particularly straightforward in this case as the only complication arises from the evaluation of the projective force $\{P\mathbf{F}_i\}_{i=1}^2$. From the form of the operator P given in (10), the latter can be done by simply removing the force averaged over all generator positions from the force corresponding to each of the generators.

4. Examples and Discussions

We now present more examples showing the local equilibria and saddle points of the CVT clustering energy given by PCVTs. We limit our attention to the case of a two dimensional unit square $[0, 1)^2 \subset \mathbb{R}^2$ being the unit cell and for simplicity, we also consider only the constant density. For better visualization, all plots of PCVTs in this section are drawn in $[0, 2)^2$ which covers a larger domain consisting of 4 unit cells. By using a combination of Lloyd’s algorithm and the shrinking dimer dynamics, we are able to obtain an extensive catalog of PCVTs. We only present a selected list of examples while a more complete analysis of the numerical findings will be presented elsewhere.

4.1. Trivial examples. It is easy to see that for any integer n of the form $n = pq$ with positive integers p and q , we may generate a uniform partition of the unit square into pq smaller but equal rectangles, with the centers of all the rectangles being the generators, see examples of such PCVTs in Figure 7.

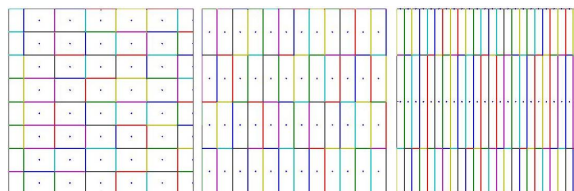


FIGURE 7. Examples of trivial PCVTs (with 12 generators in the unit cell) consisting of identical rectangular Voronoi regions.

4.2. PCVTs with a few generators in the unit cell. In Figure 8, PCVTs with three generators in the unit cell are given while in Figure 9, PCVTs with four generators in the unit cell are given. Trivial examples with the same number of generators are neglected. Configurations that can be obtained from the figures shown through a global rigid body motion in \mathbb{R}^2 , including translation, reflection and rotation, are also neglected. Similarly, in Figure 10, PCVTs with seven generators in the unit cell are given. One can see there are considerably more PCVT configurations with $n = 7$ in comparison with $n = 3$ or $n = 4$.

Note that the first plot given in either Figure 8, Figure 9 or Figure 10 corresponds to that with the lowest PCVT clustering energy. Moreover, for a given n , all of these plots are arranged in the order of increasing PCVT clustering energy.

Given the symmetry of the unit cell, it is not surprising to see many examples of PCVTs shown earlier exhibit a four-fold or other types of symmetries with respect to the spanning vectors. The latter, however, is not always the case as seen from some of the examples associated with $n = 7$. In Figure 11, additional PCVTs with 3, 4 and 6 generators in the unit cell are given for which the symmetry axes are again not directly aligned with the axis directions.

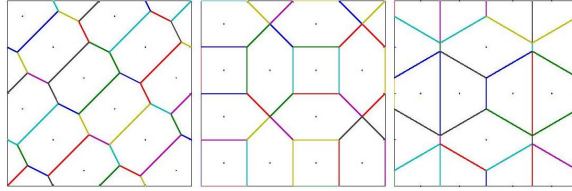


FIGURE 8. Examples of PCVTs with 3 generators in the unit cell.

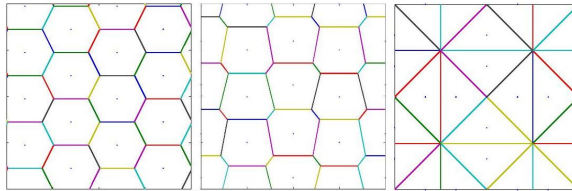


FIGURE 9. Examples of PCVTs with 4 generators in the unit cell.

4.3. PCVTs: comparison of energy. We now present some PCVT configurations that correspond to the minima of the PCVT energy. These configurations differ from each other. For several values of n (the number of generator in the unit cell), they show lattice-like structures as shown in Figure 12. For a few values of n (such as $n = 13, 14, 18$), there are no obvious simple lattice structure beyond that determined by the periodicity with respect to the unit square, see Figure 13. Note that the cases of $n = 2, 3, 4$ have been shown in earlier Figures.

We now compare how the energy of the different PCVT configurations varies. In Figure 14 we plot the energy values of a number of PCVTs with the number of generators in the unit cell ranging from $n = 1$ to $n = 10$. For each n , the plotted data points are spread around an interval near the value of n to allow better visualization. One may observe that, as n gets larger, the gaps between the energy levels associated with different PCVTs for the same given n become smaller near the lowest energy level. Moreover, there is also an increasing number of critical points sharing energy values very close to the lowest energy level associated with the global minimum PCVT configuration for each n . All of these factors contribute to the complex nature of the CVT energy landscape.

It can be rigorously shown that the minimum PCVT energy for a given number of generators in the unit cell, n , decreases monotonically to 0 as n increases to infinity. For the two dimensional case under consideration, the minimum energy is at least inversely proportional to n . Thus, in order to better assess the energy contribution when n is changing, a more suitable quantity is the minimum of the rescaled average PCVT energy per generator per unit area. Such rescaling, based on a simple dimensional analysis, can be easily done by multiplying \mathcal{K}_p by a factor of n . The values of rescaled average PCVT energy per generator per unit area are then shown in figure 15 for the minimum PCVT configurations with n ranging from 1 to 20.

One may further observe that the case $n = 15$ corresponds to a smaller rescaled energy. This is not surprising as we can see from Figure 12 that the corresponding PCVT resembles that associated to a regular hexagon lattice. The rescaled energy per unit area per generator for the minimum configuration with $n = 15$ is about

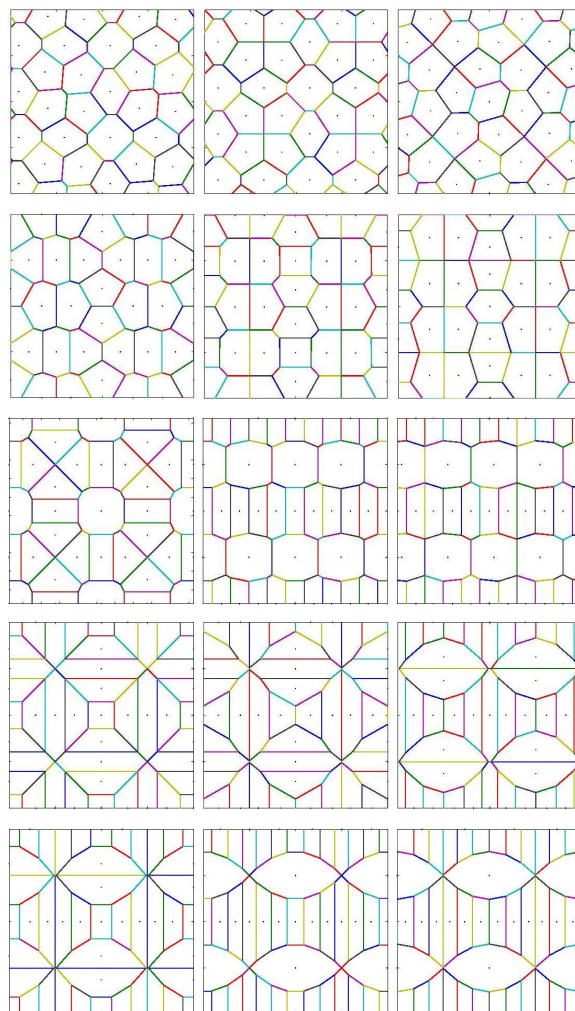


FIGURE 10. Examples of PCVTs with 7 generators in the unit cell.

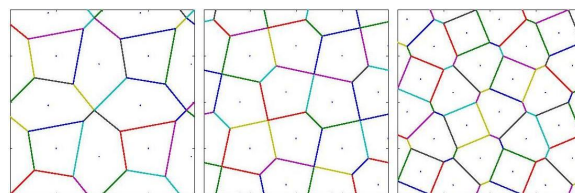


FIGURE 11. Examples of PCVTs with 3, 4 and 6 generators which are not symmetric with respect to the two axis directions.

0.160444 while the one for the perfect regular hexagon lattice is close to 0.160375. The latter configuration, according to the two dimensional version of the Gershó's conjecture [26] is the asymptotic limit of the optimal CVT configuration, a fact that has been verified in [38].

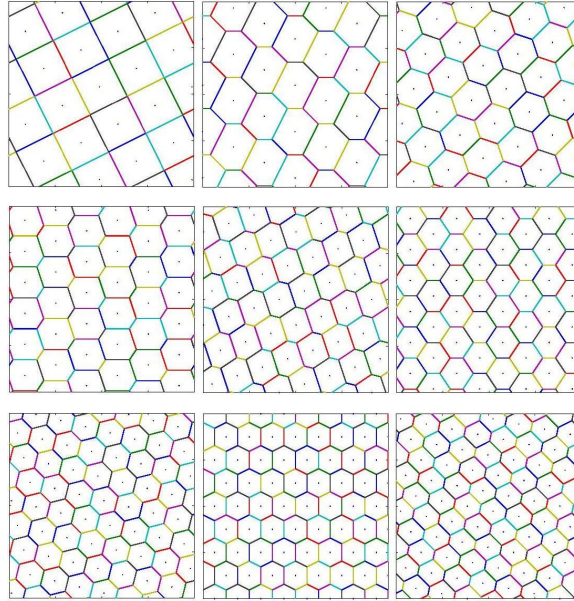


FIGURE 12. Examples of minimum energy PCVTs that enjoy simple lattice structures associated with $n = 5, 6, 8, 9, 11, 12, 15, 16$ and 19 generators in the unit cell.

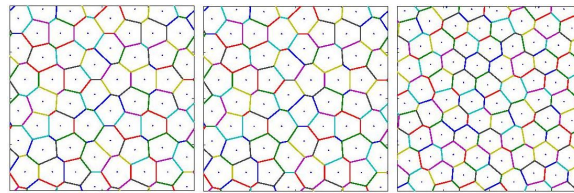


FIGURE 13. Examples of PCVTs which are the minimum energy configurations associated with $n = 13, 14$ and 18 generators in the unit cell.

4.4. Implications of the complex energy landscape. In Figure 16, a few sample PCVTs with 15 generators in the unit cell are given. These plots are arranged in the order of increasing CVT clustering energy. Though we have seen that the minimum configuration closely resembles hexagonal lattice, our computation reveals the existence of a number of other critical points of the energy. The latter contributes to the complex nature of the energy landscape and makes the search of optimal design computationally challenging. We now illustrate its implications with two examples.

As the first example, we recall that in [43], configurations with low energy values were used in the design of optimal photonic crystals. For the square unit cell, an added consideration allowed to focus only on those designs exhibiting the four fold symmetry and computational results were presented for optimal shapes (PCVTs) with the number of generators ranging from $n = 1$ to $n = 15$. While most of the results in [43] match the calculations reported here, we note a particular exception: the shape on the right of the bottom row of Figure 16 was taken as the optimal

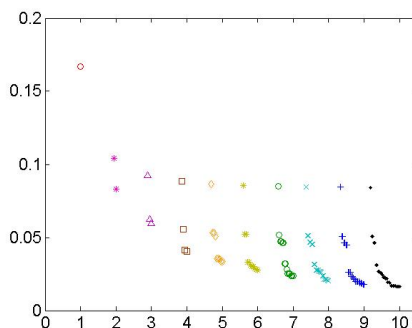


FIGURE 14. Energy values associated with various configurations with the number of generators n between 1 and 10.

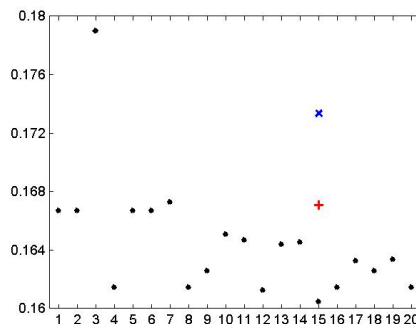


FIGURE 15. Rescaled energy values per generator per unit area for minimum PCVT configurations with n between 1 and 20. Two extra data points were added for two particular configurations with $n = 15$.

shape in [43] which corresponds to a rescaled energy value 0.173358. However, there is another design, given by the shape in the center of the middle row, which has an indubitably lower rescaled energy value 0.167097. To visualize the energy difference, in Figure 15, we also plot the rescaled energy values associated with these two configurations. This finding highlights the importance of more careful exploration of the energy landscape which might be universal in many optimal design problems [44].

As another example, we see in the Figure 13 that there are minimum energy PCVT configurations not displaying simple lattice structures even though the PCVT with the lowest energy per generator per unit area leads to the perfect hexagonal lattice. In fact, careful observations can easily reveal that in the PCVTs given in Figure 13, there are polygonal Voronoi cells having five and seven edges. This leads to the so called topological defects or scars, in contrast to hexagon cells having exactly six edges. Such a situation has been observed in many other contexts where the complex energy landscape has played a significant role [2]. Though most attention in the literature has been focused on the local minimum energy configurations, the study of saddle points may help provide a better understanding of the

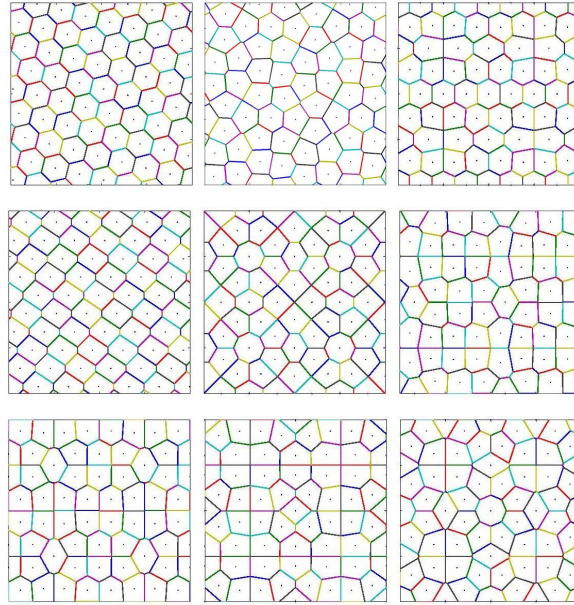


FIGURE 16. Examples of PCVTs with 15 generators in the unit cell. The configuration on the left of top row has the lowest energy while the configuration in the center of the middle row has the lowest energy among those exhibiting the four-fold symmetry.

overall energy landscape and the so-called geometrical and topological frustration exhibited in the related physical processes.

5. Conclusion

In this work, we introduced the notion of the periodic centroidal Voronoi tessellations (PCVTs) which are CVTs that exhibit certain periodicity in the Euclidean space. We also explored the relation of PCVTs with critical points of the associated CVT clustering energy. By adapting traditional algorithms for the computation of CVTs and utilizing a recently developed saddle point search algorithm based on the shrinking dimer dynamics, we developed a number of strategies for computing PCVTs. As a demonstration, we presented a number of numerically computed PCVTs associated with a constant density and a two dimensional square unit cell. Experiments with other density functions and other types of unit cells can also be carried out in a similar fashion.

Our results and discussions of PCVTs serve several objectives. First, they illustrate the complex landscape associated with the clustering energy and hence improve our understanding of the various physical or other natural processes that may be closely monitored through the clustering CVT energy. The interplay between local symmetry and global optimality associated with an energy landscape has been a fascinating topic in a number of fields (see for instance [2]), yet most of the focus in the literature has been limited to the examination of energy minimizers. The shallowness of valleys between local minimizers as identified by energy barriers at saddle points is likely to play a significant role in both numerical optimization and natural physical phenomenon.

Moreover, given the close connections between CVTs and PCVTs and in accordance with the Gersho's conjecture [19, 26] alluded to earlier in the paper, one may expect that, as the number of CVT generators grows, some PCVT-like local patterns may emerge in patches away from the boundary. Such a phenomenon could be not only of intellectual interest but also of much practical value. For instance, the dual Delaunay triangulations associated with PCVTs or large patches of PCVTs likely possess similar periodic structures so that one may end up with meshes that are unstructured globally but, to a very large extent, may enjoy some high degree of regularity locally. This would certainly be a great advantage for the CVT-based unstructured grid generation and optimization [14, 18, 20, 21]. These issues need to be investigated further, and the work presented here provides the foundation for more general studies (e.g. in higher dimensions) and perhaps for other generalized notions of CVTs that have been discussed in the literature [16].

Acknowledgment

JZ and QD are supported in part by NSF DMS-1016073. ME wants to acknowledge the support by NSF DMS-0915013 and a Ralph E. Powe Junior Faculty Enhancement Award. The authors would like to thank Professors Max Gunzburger and Lili Ju for interesting discussions on the subject.

References

- [1] P. ALLIEZ, T. DE VERDIERE, O. DEVILLERS, AND M. ISENGURG, Centroidal Voronoi diagrams for isotropic surface remeshing, *Graphic Models*, **67** (2005), pp.204-231.
- [2] A. R. BAUSCH, J. BOWICK, A. CACCIUTO, A. D. DINSMORE, M. F. HSU, D. R. NELSON, M. G. NIKOLAIDES, A. TRAVESSET AND D. A. WEITZ, Grain Boundary Scars and Spherical Crystallography, *Science*, **299** (2003), pp.1716.
- [3] E. BARNES AND N. SLOANE, The optimal lattice quantizer in three dimensions, *SIAM J. Algebraic Discrete Methods*, **4** (1983), pp.31-40.
- [4] M. CAPPELLARI AND Y. COPIN, Adaptive spatial binning of integral-field spectroscopic data using Voronoi tessellations, *Monthly Notices of the Royal Astronomical Society*, **342** (2003), pp.345-354.
- [5] Y. CHEN, Z. WANG, AND J. LIANG, Optimal dynamic actuator location in distributed feedback control of a diffusion process, *Inter. J. Sensor Networks*, **2** (2007), pp.169-178.
- [6] H. COHN, Order and disorder in energy minimization, in *Proceedings of the International Congress of Mathematicians Hyderabad, India*, (2010).
- [7] J. CORTES, S. MARTINEZ, T. KARATAS, AND F. BULLO, Coverage control for mobile sensing networks, *IEEE Trans. Robotics and Automation*, **20** (2004), pp.243-255.
- [8] G. M. CRIPPEN AND H. A. SCHERAGA, Minimization of Polypeptide Energy XI. The method of Gentlest Ascent, *Archives of biochemistry and biophysics*, **144** (1971), pp.462-266.
- [9] O. DEUSSEN, S. HILLER, C. VAN OVERVELD, AND T. STROTHOTTE, Floating points: A method for computing stipple drawings, *Comput. Graph. Forum*, **19** (2000), pp.41-50.
- [10] Q. DU AND M. EMELIANENKO, Acceleration schemes for computing the centroidal Voronoi tessellations, *Numer. Linear Alg. Appl.*, **13** (2006), pp.173-192.
- [11] Q. DU AND M. EMELIANENKO, Uniform convergence of a nonlinear energy-based multilevel quantization scheme via centroidal Voronoi tessellations, *SIAM J. Numer. Anal.*, **46** (2008), pp.1483-1502.
- [12] Q. DU, M. EMELIANENKO AND L. JU, Convergence of the Lloyd algorithm for computing centroidal Voronoi tessellations, *SIAM J. Numer. Anal.*, **44** (2006), pp.102-119.
- [13] Q. DU, V. FABER, AND M. GUNZBURGER, Centroidal Voronoi tessellations: Applications and algorithms, *SIAM Review*, **41** (1999), pp.637-676.
- [14] Q. DU AND M. GUNZBURGER, Grid generation and optimization based on centroidal Voronoi tessellations, *Applied Math. Comput.*, **133** (2002), pp.591-607.
- [15] Q. DU AND M. GUNZBURGER, Centroidal Voronoi tessellation based proper orthogonal decomposition analysis, *Control and Estimation of Distributed Parameter Systems*, Birkhauser, Basel, 2003, pp.137-150.

- [16] Q. DU, M. GUNZBURGER AND L. JU, Advances in studies and applications of centroidal Voronoi tessellations, *Numer. Math. Theo. Meth. Appl.*, **3** (2010), pp.119-142,
- [17] Q. DU, M. GUNZBURGER, L. JU, AND X.-Q. WANG, Centroidal Voronoi tessellation algorithms for image compression, segmentation and multichannel restoration, *J. Math. Imaging Vision*, **24** (2006), pp.177-194.
- [18] Q. DU AND D. WANG, Tetrahedral mesh generation and optimization based on centroidal Voronoi tessellations, *Int. J. Numer. Methods Engrg.*, **56** (2003), pp.1355-1373.
- [19] Q. DU AND D. WANG, On the optimal centroidal Voronoi tessellations and the Gersho's conjecture in the three dimensional space, *Comput. Math. Appl.*, **49** (2005), pp.1355-1373.
- [20] Q. DU AND D. WANG, Mesh optimization based on centroidal Voronoi tessellations, *Inter. J. Numer. Anal. Model.*, **2** (2005), pp.100-114.
- [21] Q. DU AND D. WANG, Recent progress in robust and quality Delaunay mesh generation, *J. Comput. Appl. Math.*, **195** (2006), pp.8-23.
- [22] Q. DU AND J. ZHANG, Shrinking dimer dynamics and its applications to saddle point search, submitted to *SIAM J. Numer. Anal.*, 2011.
- [23] Q. DU AND J. ZHANG, Constrained Shrinking dimer dynamics for saddle point search with constraints, preprint, 2011.
- [24] W. E AND X. ZHOU, The Gentlest Ascent Dynamics, *Nonlinearity*, **24** (2011), pp.1831-1842.
- [25] M. EMELIANENKO, L. JU AND A. RAND, Nondegeneracy and weak global convergence of the Lloyd algorithm in \mathbb{R}^d , *SIAM J. Numer. Anal.*, **46** (2008), pp. 1423-1441.
- [26] A. GERSHO, Asymptotically optimal block quantization, *IEEE Trans. Inform. Theory*, **25** (1979), pp.373-380.
- [27] A. GERSHO AND R. GRAY, *Vector Quantization and Signal Compression*, Kluwer, Boston, 1992.
- [28] A. GUESSAB AND E. CHMEISSERR, Construction of positive definite cubature formulae and approximation of functions via Voronoi tessellations, *Adv Comput Math*, **32** (2010), pp.25-41.
- [29] H. HELLWIG, M. JESCHKE, AND O. DEUSSEN, A contact pressure model based on centroidal Voronoi diagrams for surfaces of revolution, *Proceedings of the Fifth Annual Inter. Symp. Voronoi Diagrams Sci. Engr.*, 2008.
- [30] G. HENKELMAN AND H. JONSSON, A dimer method for finding saddle points on high dimensional potential surfaces using only first derivatives, *Journal of Chemical Physics*, **111** (1999), pp.7010-7022.
- [31] S. Hiller, H. Hellwig, and O. Deussen, Beyond stippling – methods for distributing objects on the plane, *Computer Graphics Forum*, **22** (2003), pp.515-522.
- [32] L. JU, Q. DU, AND M. GUNZBURGER, Probabilistic methods for centroidal Voronoi tessellations and their parallel implementations, *Parallel Comput.*, **28** (2002), pp.1477-1500.
- [33] J. KIEFFER, Uniqueness of locally optimal quantizer for log-concave density and convex error function, *IEEE Trans. Infor. Theory*, **29** (1983), pp.42-47.
- [34] Y. LIU, W. WANG, B. LEVY, F. SUNG, AND D-M. YAN, On centroidal Voronoi tessellation - Energy smoothness and fast computation, *ACM Trans. Graphics*, **28** (2009), pp.1-17.
- [35] S. LLOYD, Least squares quantization in PCM, *IEEE Trans. Inform. Theory*, **28** (1982), pp.129-137.
- [36] L. LU, B. LEVY AND W. WANG, Centroidal Voronoi tessellation of line segments and graphs, INRIA-ALICE Technical report, 2009.
- [37] M. MORIGUCHI AND K. SUGIHARA, Constructing centroidal Voronoi tessellations on surface meshes, *Studies in Computational Intelligence*, **158** (2009), pp.235-245.
- [38] D. NEWMAN, The hexagon theorem, *IEEE Trans. Inform. Theory*, **28** (1982), pp.137-139.
- [39] A. OKABE, B. BOOTS, K. SUGIHARA, AND S. CHIU, *Spatial Tessellations: Concepts and Applications of Voronoi Diagrams*, 2nd edition, Wiley, Chichester, 2000.
- [40] Y. OUYANG, Design of vehicle routing zones for large-scale distribution systems, *Transportation Research B: Methodological*, **41** (2007), pp.1079-1093.
- [41] G. RONG, Y. LIU, W. WANG, X. YIN, X. GU AND X. GUO, GPU-Assisted Computation of Centroidal Voronoi Tessellation, *IEEE Transactions on Visualization and Computer Graphics*, **17** (2011), pp.345-356
- [42] Y. SAKA, M. GUNZBURGER, AND J. BURKARDT, Latinized, improved LHS, and CVT point sets in hypercubes, *Int. J. Numer. Anal. Model.*, **4** (2007), pp.729-743.
- [43] O. SIGMUND AND K. HOUGAARD, Geometric Properties of Optimal Photonic Crystals, *Physical Review Letters*, **100** (2008), 153904
- [44] S. TORQUATO, Optimal Design of Heterogeneous Materials, *Annual Review of Materials Research*, **40** (2010), pp.101-129.

- [45] J. WANG, L. JU AND X. WANG, An Edge-Weighted Centroidal Voronoi Tessellation Model for Image Segmentation, *IEEE Transactions on Image Processing*, **18** (2009), pp.1844-1858.
- [46] S. VALETTE AND J. CHASSERY, Approximated centroidal Voronoi diagrams for uniform polygonal mesh coarsening, *Computer Graphics forum*, **23** (2004), pp.381-389.

Department of Mathematics, Pennsylvania State University, University Park, PA 16802, USA
E-mail: j.zhang@math.psu.edu

Department of Mathematical Sciences, George Mason University, Fairfax, VA 22030, USA
E-mail: memelian@math.gmu.edu
URL: math.gmu.edu/~memelian

Department of Mathematics, Pennsylvania State University, University Park, PA 16802, USA
E-mail: qdu@math.psu.edu
URL: www.math.psu.edu/qdu